Naval Research Laboratory

Washington, DC 20375-5320

NRL/FR/5712--19-10,335

Autonomous Soaring across Three Orders of Magnitude of Mass

DANIEL J. EDWARDS
AARON D. KAHN

Offboard Countermeasures
Tactical Electronic Warfare Division

BLAKE POE

Soaring Laboratories, Inc.
Boulder, CO

August 2, 2019

REPORT DOCUMENTATION PAGE

Form Approved
OMB No. 0704-0188

PLEASE DO NOT RETURN YOUR FORM TO THE ABOVE ORGANIZATION.

1. REPORT DATE *(DD-MM-YYYY)*	2. REPORT TYPE	3. DATES COVERED *(From - To)*
02-08-2019	NRL Formal Report	December 2017 - December 2018

4. TITLE AND SUBTITLE
Autonomous Soaring across Three Orders of Magnitude of Mass

5a. CONTRACT NUMBER

5b. GRANT NUMBER

5c. PROGRAM ELEMENT NUMBER

6. AUTHOR(S)
Daniel J. Edwards, Aaron D. Kahn, and Blake Poe*

5d. PROJECT NUMBER
57-6874-A8

5e. TASK NUMBER

5f. WORK UNIT NUMBER
6874

7. PERFORMING ORGANIZATION NAME(S) AND ADDRESS(ES)
Naval Research Laboratory
4555 Overlook Ave SW
Washington, DC 20375-5320

8. PERFORMING ORGANIZATION REPORT NUMBER
NRL/FR/5712--19-10,335

9. SPONSORING/MONITORING AGENCY NAME(S) AND ADDRESS(ES)
Naval Research Laboratory
4555 Overlook Ave SW
Washington, DC 20375-5320

10. SPONSOR/MONITOR'S ACRONYM(S)
NRL

11. SPONSOR/MONITOR'S REPORT NUMBER(S)

12. DISTRIBUTION/AVAILABILITY STATEMENT
Approved for public release; distribution is unlimited

13. SUPPLEMENTARY NOTES
*Soaring Laboratories, Inc, 4184 Greenbriar Blvd., Boulder, CO 80305-7074

14. ABSTRACT

Autonomous soaring extracts energy from the environment to improve aircraft endurance. It does so by gaining altitude in the convective boundary layer. This technique has been tested on two aircraft that are three orders of magnitude apart in mass (0.410kg to 710kg), showing the technique's general applicability. Despite three orders of magnitude difference in weight, both aircraft showed successful closed-loop autonomous soaring guidance. In the smaller unmanned aircraft, the autopilot closed the guidance loop; in the manned aircraft, the pilot closed the guidance loop using commands from a flight director application called ThermalFinder. Both aircraft showed similar autonomous soaring behaviors. In addition, the updraft sensing described in this report is unaffected by inclusion of a propulsion system using a few simple tuning parameters, thereby widening the method's general applicability to other aircraft. Autonomous soaring holds great potential to increase endurance (and range) or reduce fuel consumption of soaring aircraft.

15. SUBJECT TERMS

autonomous soaring	UAV	ALOFT
soaring	swarm	ISR

16. SECURITY CLASSIFICATION OF:			17. LIMITATION OF ABSTRACT	18. NUMBER OF PAGES	19a. NAME OF RESPONSIBLE PERSON
a. REPORT	b. ABSTRACT	c. THIS PAGE			Daniel J. Edwards
U/U	U/U	U/U	U/U	18	19b. TELEPHONE NUMBER *(Include area code)* 202-404-7623

Reset

Standard Form 298 (Rev. 8/98)
Prescribed by ANSI Std. Z39.18

This page intentionally left blank

CONTENTS

This page intentionally left blank

EXECUTIVE SUMMARY

Autonomous soaring extracts energy from the environment to improve aircraft endurance. It does so by gaining altitude in the convective boundary layer. This technique has been tested on aircraft of varying masses. In addition, by using a few simple tuning parameters, the updraft sensing described in this report is unaffected by inclusion of a propulsion system, thereby widening the method's general applicability to other aircraft. This report presents flight-testing results of the same autonomous soaring math on two aircraft.

These aircraft, one with a mass of 0.41 kg and the other of 710 kg, were flight tested with the same autonomous soaring algorithms. Despite three orders of magnitude difference in weight, both aircraft demonstrated successful closed-loop autonomous soaring guidance. In the smaller unmanned aircraft, the autopilot closed the guidance loop; in the manned aircraft, the pilot closed the guidance loop using commands from a flight director application called ThermalFinder. Both aircraft showed similar autonomous soaring behaviors.

The variometer math that estimates vertical wind speed was discovered to be overcompensated in the 710 kg aircraft (it showed inverse "stick thermal" response) and tracked down to an angle-of-attack estimate exacerbated by a linear multiplier on airspeed. However, steady-state performance was shown to have less time lag than a traditional variometer, and was unaffected by motor on/off state or glide polar changes.

These flights show the applicability of the soaring algorithms to solar-battery-electric- and internal combustion engine-powered flight. The variometer and thermal identification algorithms are the key elements of this system. Implementation varies to suit the size and capability of the aircraft. Autonomous soaring holds great potential to increase endurance (and range) or reduce fuel consumption of soaring aircraft. These techniques have now been demonstrated to be applicable to aircraft of various sizes.

This page intentionally left blank

AUTONOMOUS SOARING ACROSS THREE ORDERS OF MAGNITUDE OF MASS

INTRODUCTION

Autonomous soaring is a technique that extracts energy from the vertical wind motions of the atmosphere, such as from convective thermal updrafts. The aircraft uses software to sense, identify, and guide itself into energy-positive areas, gaining energy to produce increased range or endurance [2]. Soaring can be done by orbiting in lift to gain altitude, or done in a straight-line using dolphin soaring techniques (e.g., speed-to-fly).

Several experiments in academia, industry, and the defense sector have demonstrated performance gains using autonomous soaring techniques. A 7 kg mass and 4.2 m wingspan SBXC aircraft (RnR Products) was used by Edwards, Allen, Depenbush, and Andersson [1–4]. The SBXC had flights of more than 5 hours and over 70 miles range as a sailplane [5], and more than 11 hours as a solar-electric in combination with a solar battery recharging system [6]. It also performed experiments with cooperative autonomous soaring [7]. A 1.2 kg mass, 3 m wingspan aircraft named Sky Sailor was used for some soaring simulation, though results were only minor improvements in endurance [8]. On the large scale, a 17 kg and 6.5 m wingspan aircraft named Ion Tiger demonstrated a doubling of battery-only endurance despite range and altitude mission constraints, limiting the available working volume for the autonomous soaring algorithms [9].

All prior experimentation had been in a relatively narrow range of aircraft mass, from 1.2 kg to 17 kg. The purpose of this report is to describe flight testing that expands the range of aircraft masses tested with these soaring algorithms by two orders of magnitude. The mathematics are unchanged across this expansion of aircraft mass range and inclusion/omission of a propulsion system. Only simple measurements and a few tuning parameters are used to tailor the algorithms for different aircraft.

The next section describes flight testing with a 0.41 kg aircraft, the following section describes flight testing with a 710 kg aircraft, and the last section draws some conclusions about the testing.

MICRO SOLAR SAILPLANE: “SOLAR AURORA”

Hardware

The Naval Research Laboratory (NRL) developed a 410 g solar-battery micro glider with a 1.5 m wingspan, derived from a commercial electric discus launch glider (Ultegra Elektro from Strat Air Modeltechnik Gmbh, Austria) with a custom solar-integrated wing. Figure 1 shows the aircraft and Table 1 shows the major parameters used for the soaring software.

Manuscript approved July 8, 2019.

Fig. 1—NRL's Solar Aurora showing the wing-integrated solar array (left) and at altitude while soaring (right)

Table 1—Solar Aurora Major Parameters Needed for the ThermalFinder Application

Term	Value	Unit	Notes
Span	1.5	m	Aircraft wingspan
Area	0.225	m^2	Aircraft wing area
Aspect Ratio	10.0 : 1	-	Wing aspect ratio
Airfoil	Zone V2 modified	-	-
Empty Weight	0.41	kg	Weight of empty aircraft
Gross Weight	0.41	kg	Weight including fuel and passengers
CL_0	0.15	-	Coefficient of lift at zero alpha
CL_a	5.02	-	Coefficient of lift per degree alpha
CY_{beta}	-0.55	-	Coefficient of side force per degree beta
$W_{Z,latch}$	1.3	m/s	Vertical wind speed latch user parameter
T_{latch}	25	s	Time to latch user parameter

SunPower (San Jose, CA) monocrystalline silicon cells were diced into thirds, bussed together in series, and laminated into an array. This array was co-molded into a composite wing structure using compression molding of a solid foam core and fiberglass/carbon composite skins. Final wing efficiency was measured as 14% (percent) at Standard Test Conditions (STC) on the earth's surface at an air mass factor of 1.5 (AM1.5), producing approximately 15 W of 20 W needed for sustained flight. A lithium polymer battery of 2.2 Wh (2-series, 300 mAh) provides approximately 15 minutes of endurance when not using the solar system. The aircraft is hand-launched and belly-landed in short grass.

A custom power management system provides the ability to recharge when excess solar energy is available and powers aircraft navigation and guidance electronics. A custom autopilot consists of an Atmel microcontroller, Global Positioning System (GPS) receiver, 3-axis gyro/accelerometer, and dynamic/static pressure sensors. The autopilot and power management hardware are tightly integrated.

Software

The autopilot software is a custom NRL design. Basic airspeed, altitude, and heading controllers provide GPS waypoint guidance. Additionally, autonomous soaring software has been written for this autopilot's remaining processor resources.

Wind is estimated using the method described in Kahn [10] that determines the vertical wind even if the propulsion system is providing thrust input. With wind, a thermal estimation algorithm based on the algorithm in Kahn [10] finds any nearby thermals using a typical Gaussian model [11]. Finally, mode logic switches the aircraft between two states: soaring or waypoint guidance. These soaring algorithms are all layered on top of standard autopilot control loops and constitute "autonomous soaring."

Baseline Flight Testing

The baseline flight test was to measure the battery-only endurance of the aircraft. This testing took place on March 16, 2018, an overcast day with low winds and poor soaring conditions. The aircraft was flown manually by an expert pilot starting with a freshly charged battery and the solar wing input disconnected. A smooth flight at very low altitudes (<10 m) measured the battery-only endurance at 15 minutes.

Soaring Flight Testing

This test occurred on March 9, 2018, in mostly sunny and good soaring conditions. The battery was fully charged at launch. After manually climbing to altitude, the autopilot was engaged to hold a box flight pattern. Soaring mode was enabled, allowing the autopilot to latch onto and track any thermals found along the route.

Despite a 15 minute battery-only endurance, the solar/soaring flight exceeded 3.1 hours and the aircraft landed with the battery nearly fully charged at 8.2 V. Multiple thermals carried the aircraft to its maximum limits several times. The flight was ended due to range availability constraints, not aircraft energy limitations or environmental changes.

The aircraft was programmed to follow the nominal holding box. A minimum altitude of 225 m (±10 m) was enforced by running the motor. If the algorithm sensed a nearby thermal, it steered the aircraft toward the estimated center. This allowed the UAV to orbit in the most likely area of lift. If the aircraft exceeded a maximum altitude of 550 m while soaring or exceeded a user-set range from the ground station, the soaring would automatically disengage and the aircraft would return to the holding box. The motor remained off any time the vehicle was above the minimum altitude.

Figure 2 shows the altitude time history of the flight. Red indicates when the autonomous soaring mode was enabled and actively latched into a thermal. Black indicates when the soaring mode was disabled or the soaring system was not actively latched into a thermal. The data shows five major thermal climbs of more than 100 m and several smaller thermals above the minimum altitude. The highest altitude achieved was 850 m and the longest no-motor period was 16 minutes. Note that the very steep dives at 90 minutes and 150 minutes were manual descents with full flaperons to scrub off the altitude, as the aircraft was at the edge of visual line of sight.

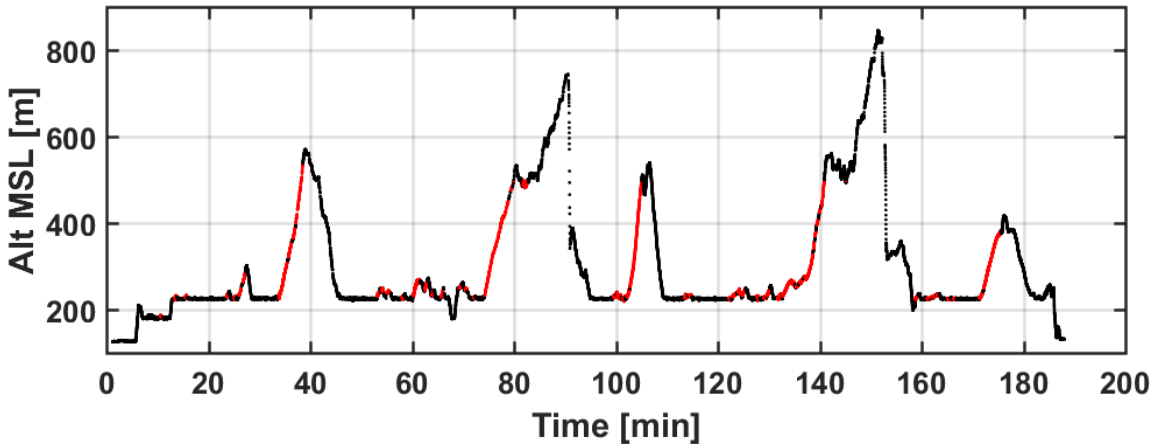

Fig. 2—Solar Aurora altitude time history for August 9, 2018 flight (red is actively-latched soaring)

Figure 3 shows the battery voltage time history over the same flight. Full charge on the 2-series cells is 8.4 V, the minimum acceptable voltage is 7.0 V, and the charger's programmed maximum voltage was 9.0 V. The data shows takeoff with a full battery charge, a drop in voltage for the climb to altitude, then intermittent charge and discharge cycles. The battery exceeded its pre-takeoff voltage 83 minutes into the flight, then nearly reached full charge at the landing at 187 minutes after takeoff.

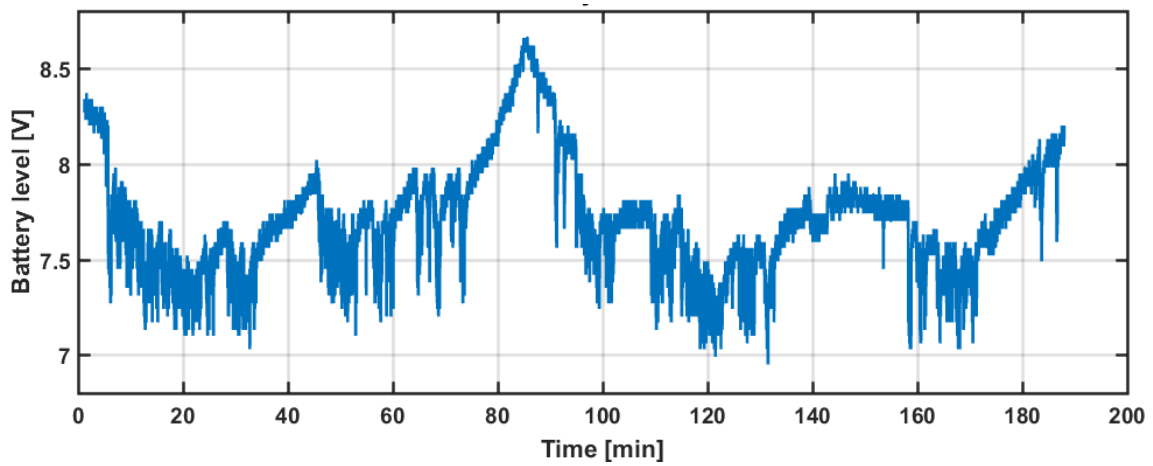

Fig. 3—Solar Aurora battery time history for August 9, 2018 flight

Figure 4 shows the flight path of the Solar Aurora with colors indicating altitude. The holding box is somewhat visible beneath the higher altitude soaring orbits. The sections of drifting turns are the autonomous soaring events. Interestingly, the direction of drift of the thermals (observed by the average direction of the orbits) was inconsistent throughout the day as the ambient wind direction shifted.

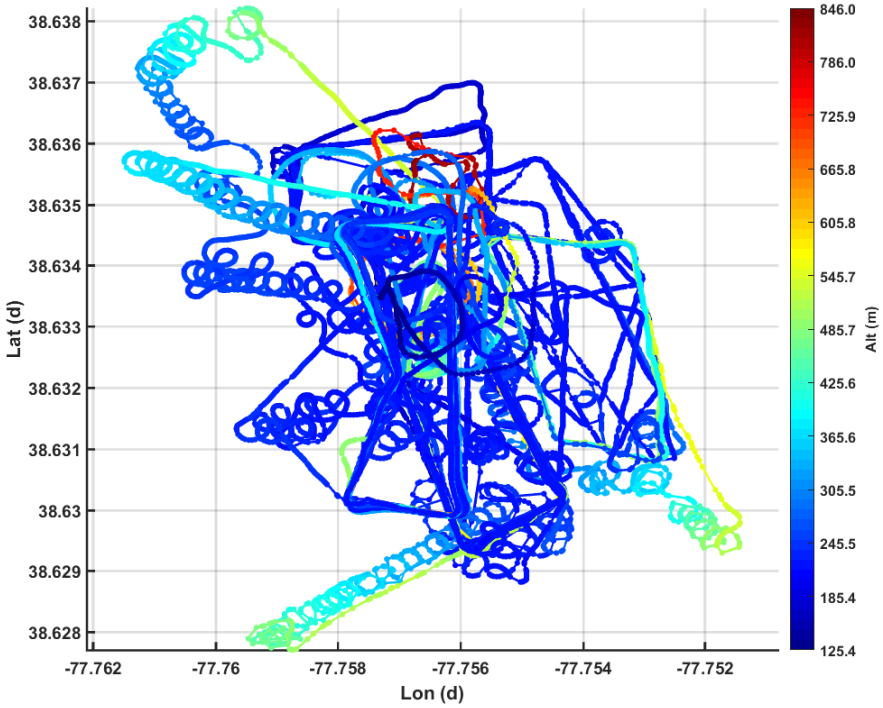

Fig. 4—Solar Aurora 3D flight path for solar-soaring flight August 9, 2018

MANNED MOTOR-GLIDER: "SUPER DIMONA"

Hardware

A standard dual-seat taildragger Super Dimona (Diamond Aircraft Gmbh, Austria) motor-glider of 16 m wingspan and 710 kg gross weight (shown in Fig. 5) was modified for experimentation, with autonomous soaring algorithms acting as a flight director for the human pilot.

Fig. 5—Super Dimona N351HK used for soaring experiments (left) and view while flying (right)

A stock Piccolo Nano (Cloud Cap Technologies, Hood River, OR) was installed behind the instrument panel and connected to the stock air pressure system. A GPS antenna was mounted on top of the Piccolo and a small lithium battery provided power for these two electronics.

A tablet running Windows 10 operating system and the custom NRL ThermalFinder application used the Piccolo's navigation solution, ran the autonomous soaring algorithms, and provided a graphical user

interface (GUI) for the pilot to follow. Fig. 5 shows the tablet in the co-pilot's right hand. Table 2 shows the parameters needed for the application.

Table 2—Super Dimona Major Parameters Needed for the ThermalFinder Application

Term	**Value**	**Unit**	Notes
Span	16	m	Aircraft wingspan
Area	15.24	m^2	Aircraft wing area
Aspect Ratio	16.8 : 1	-	Wing aspect ratio
Airfoil	Wortmann FX 63-137	-	-
Empty Weight	561	kg	Weight of empty aircraft
Gross Weight	710	kg	Weight including fuel and passengers
CL_0	0.6	-	Coefficient of lift at zero alpha
CL_a	5.8	-	Coefficient of lift per degree alpha
CY_{beta}	-0.5	-	Coefficient of side force per degree beta
$W_{Z,latch}$	2.3	m/s	Vertical wind speed latch user parameter
T_{latch}	20	s	Time to latch user parameter

Software

The NRL ThermalFinder application has four major modules:

1. Communications interface with the autopilot
2. Vertical wind estimator (variometer)
3. Thermal identification and localization
4. Graphical user interface

The communication system will not be covered in this report, as this is specific to the selected autopilot source, used here simply for its navigation solution.

The vertical wind estimator and thermal identification have been described in Kahn [10]. The mathematics behind these modules is identical to the implementation in the Solar Aurora described earlier.

Since the vehicle is a stock manned motor-glider without servo actuators that can operate the control surfaces, a flight director paradigm was selected as a reasonable analogy for autonomous soaring control. The interface, shown in Fig. 6, provides both a time history of the variometer and orbit guidance for the pilot to follow.

Fig. 6—NRL ThermalFinder GUI screenshot. The variometer time history plot is shown in the upper section of the window. The lower section shows an aircraft-centric view with a thermal indicated behind and to the right of the aircraft.

Flight Testing

Several test flights occurred between February 20 and July 29, 2018, in California, Nevada, and Utah under different environmental conditions. These flights tested the ThermalFinder application over the Pacific Ocean, over rural Orange County and the dry Santa Ana mountains, in the mountain wave of the Sierra Nevada, and in strong desert thermals near Parowan, Utah (Fig. 7). This section does not describe each flight in detail, but rather gives general observations that held across all flights and discusses some specific case studies.

Fig. 7—Tailcam shot of the Super Dimona soaring somewhere pretty

Variometer

The variometer (vario) time history strip chart was examined during flight in both calm and turbulent conditions. The ThermalFinder vario did not show bias with the motor running at full or idle, or at airspeed from 50 to 90 kts, verified in smooth air above the Pacific Ocean. This confirms the assertion of estimating the vertical winds directly, regardless of motor contribution or drag polar.

ThermalFinder was flown on July 29 from Corona Municipal Airport to John Wayne Airport via the Ortega Mountains and Santiago Peak. The objectives of the flight were to perform a pull-up, push-over maneuver to check vario compensation, engage some thermals, and observe ThermalFinder vario compared to the Borgelt B50 vario installed in the aircraft.

The ThermalFinder variometer appears to track well with the Borgelt B50 variometer in calm, unaccelerated conditions. However, it appears to be overcompensated during maneuvers. The vario shows sink when pulling up (stick lift), and vice versa. This has been traced back to estimation of angle of attack based on autopilot attitude data. Vertical wind is linearly sensitive to bias at increasing airspeeds. At the ~100 kt airspeed of the Super Dimona, slight errors in the estimated angle of attack result in 1 to 2 m/s apparent bias. This alpha estimate issue is most evident during accelerated maneuvers.

The pilot observed that the vario functioned well overall, despite being slightly overcompensated to accelerated maneuvers. The pilot also noted how wonderful it was to have unbiased variometer during periods of straight-line flight while running the motor, thus enabling powered dolphin soaring.

Flight in Wave Lift

ThermalFinder was flown on April 14, 2018, from Fox Field in Lancaster, California to Minden, Nevada along the crest of the Eastern Sierra in light mountain wave conditions. While power settings were varied throughout the flight, ThermalFinder's indicated rate of climb correlated well with the Borgelt B50 and the climb rate of the altimeter. Climb rates were in the range of ±2knots. The ThermalFinder variometer value was more accurate than the installed B50 as it is not affected by engine throttle setting.

The thermal center indication was ignored during wave flight due to the differing shape between an assumed circular convective thermal versus the more linear wave lift region.

Case Study

To highlight ThermalFinder being flown in a 710-kg motor-glider (the Super Dimona), an example of it being flown in a specific thermal is presented.

A time-synced replay of recorded data and video permits cross-correlation between the different instruments. Telemetry data was recorded on the uncompensated Oudie variometer and displayed in SeeYou soaring software. A video camera was attached to the horizontal tail of the aircraft looking forward over the fuselage. Finally, telemetry data from the Piccolo autopilot was recorded and replayed by the ThermalFinder display. All data sources were time-synced in Figs. 8–14. The pilot's observations annotate several snapshots in time.

Figure 8 shows the general layout of the subsequent case studies. The Oudie IGC data playback is shown as aircraft steam gauges for altitude, variometer, and indicated airspeed in the upper left. The Oudie IGC data is also shown in an altitude trace and elevation plot on the bottom. The ThermalFinder display replays saved Piccolo autopilot data, shown in the upper-middle red box. Finally, the tail-cam video is shown in the upper right, and is mostly for situational awareness.

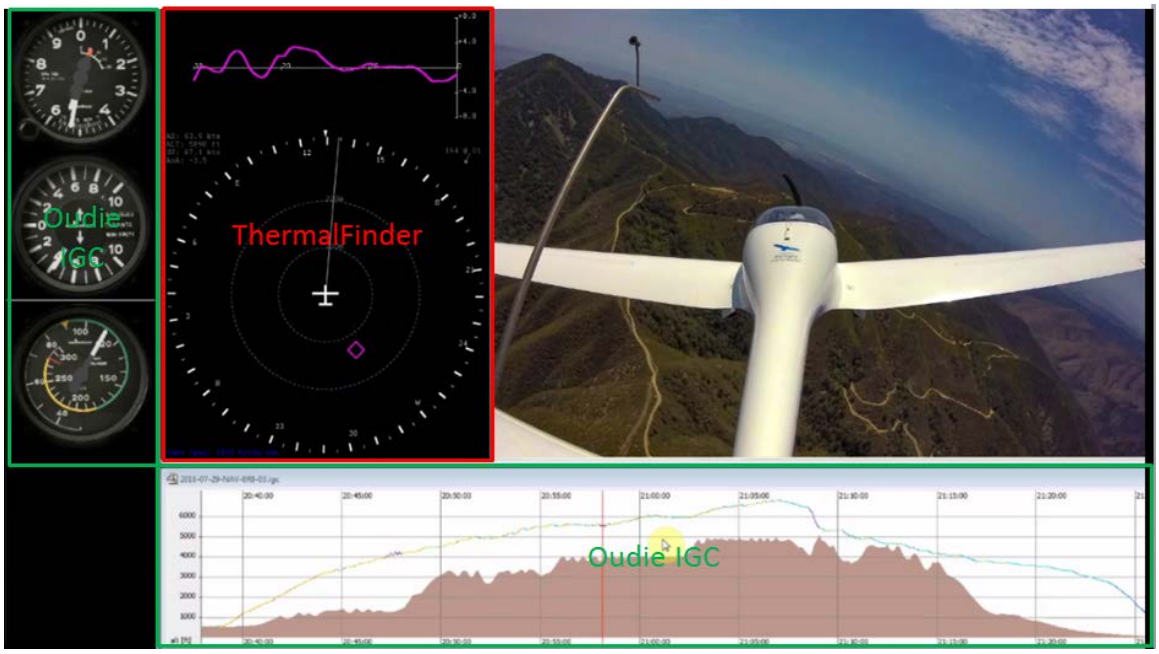

Fig. 8—ThermalFinder GUI boxed in red, Oudie IGC along left and bottom edge

Figure 9 shows the ThermalFinder just latching onto a thermal. This is indicated to the pilot with a magenta circle. As the aircraft flies, the green line points toward the center of the thermal relative to the aircraft nose.

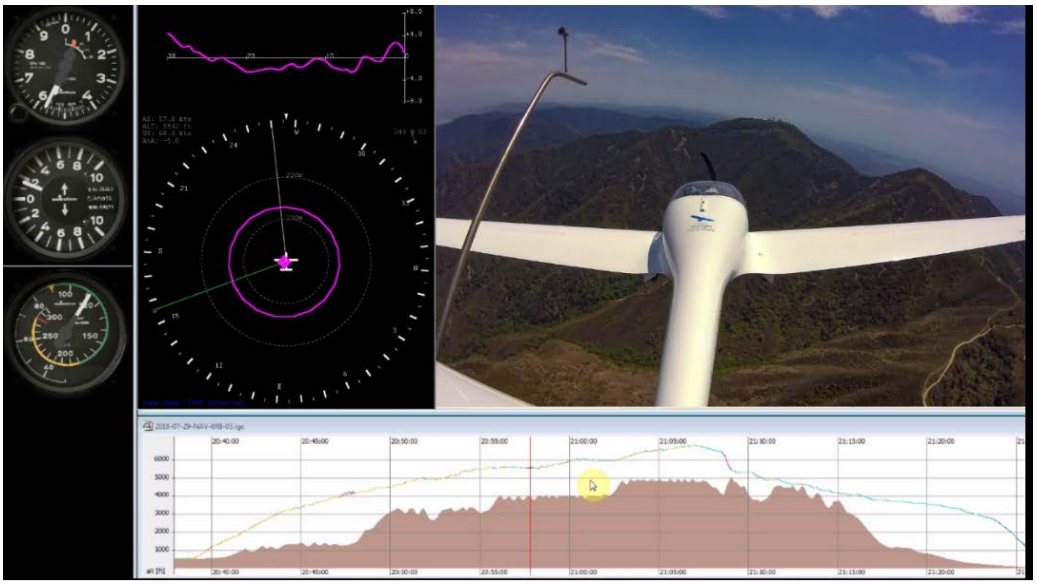

Fig. 9—ThermalFinder latching as the Dimona flies through a thermal. The ThermalFinder orbit recommendation is shown as a magenta circle on top of the aircraft.

Figure 10 shows ThermalFinder a few seconds after the latch indication from Fig. 9. The ThermalFinder display now shows the thermal behind and to the right of the aircraft. The pilot happened to start circling to the left. The Oudie and ThermalFinder varios show good agreement of lift around 1.5 to 3 knots.

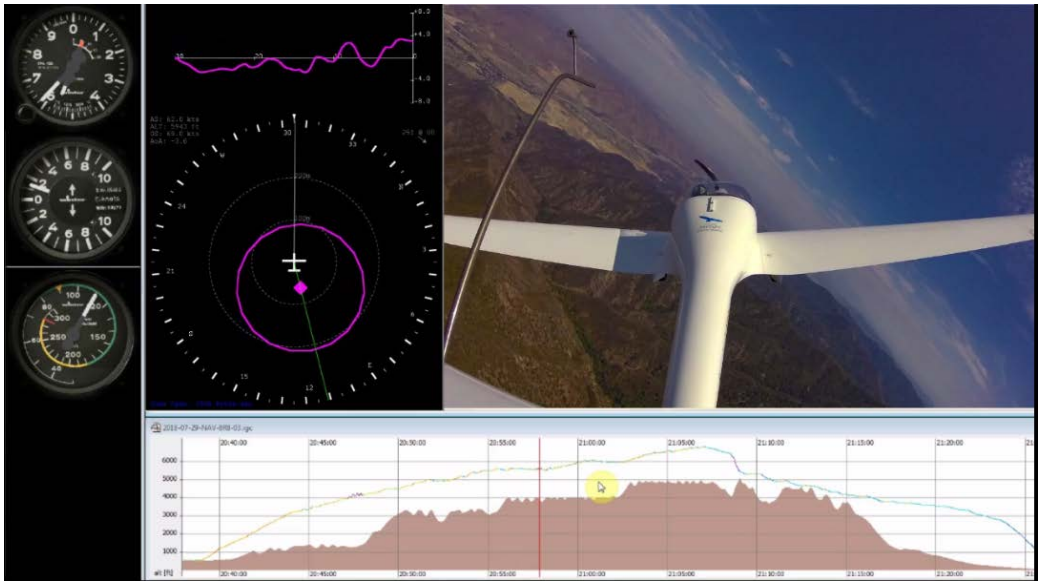

Fig. 10—Several seconds after the previous figure, ThermalFinder is still latched with the thermal center estimate behind the aircraft

In Figure 11, ThermalFinder has unlatched from the thermal. As the vario time trace shows along the top of the ThermalFinder GUI, the vario reading has been under 0 knots (indicating sink) for several seconds. When ThermalFinder unlatches, it continues to show the estimated thermal center for several seconds as it maintains a lock on the location even as the pilot flies away.

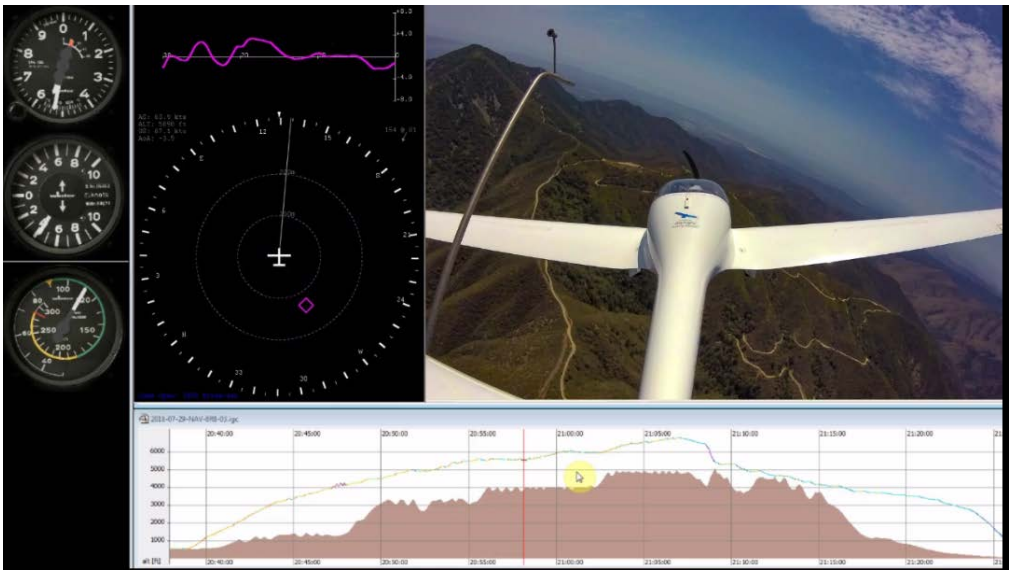

Fig. 11—After several circles the lift tapered off and ThermalFinder unlatched. The estimated thermal center is still being displayed as the magenta diamond.

Figure 12 shows ThermalFinder indicating thermals without lag whereas the Oudie vario has an approximately one second lag. The ThermalFinder vario trace maxed out around 7+ knots while the Oudie indicates 6+ knots a second later. ThermalFinder is indicating the thermal behind the aircraft to the left this time.

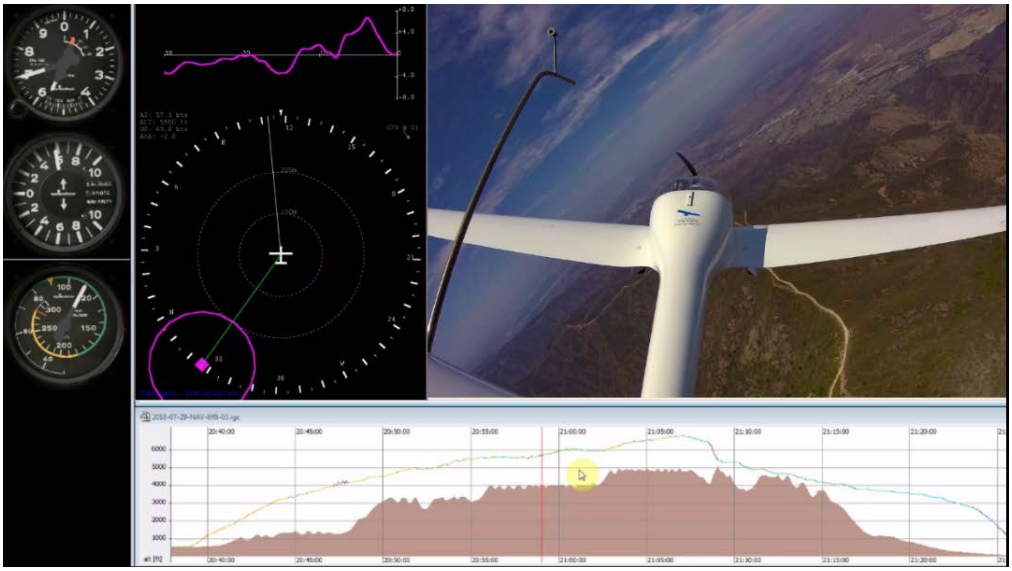

Fig. 12—ThermalFinder showing 7 knots (peak) lift, which agrees well with the time-delayed Oudie vario indicating 6 knots

Figure 13 shows ThermalFinder just after latching onto a thermal estimated to be off the right wing. The pilot's action from here would be to immediately start circling to the right and attempt to keep the thermal center directly off the right wing for proper centering. Note that the Oudie and ThermalFinder varios are in good agreement when considering the lag of Oudie.

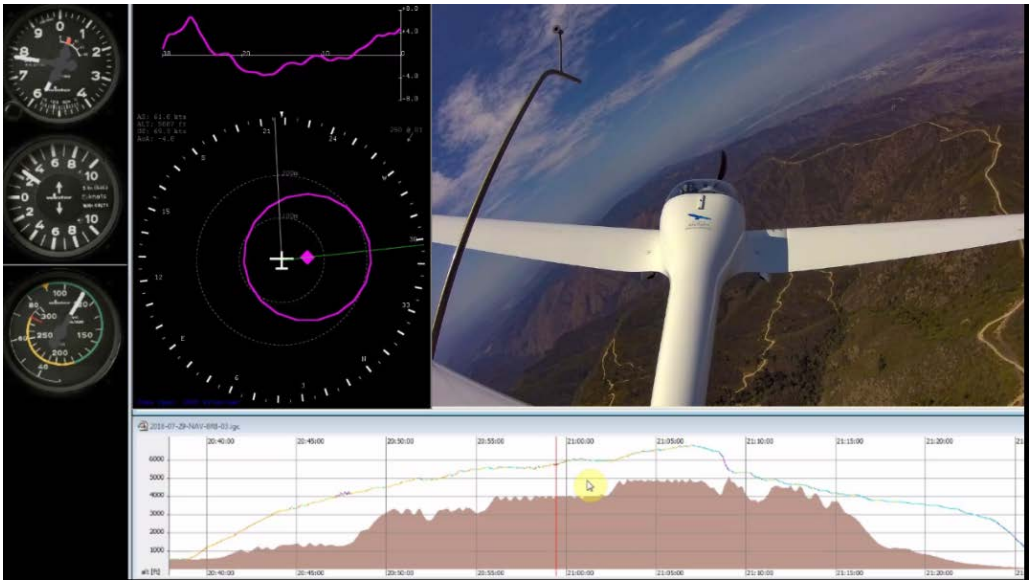

Fig. 13—ThermalFinder showing 4 knots lift, which agrees well with the time-delayed Oudie vario

Although the thermal center is often shown to be behind the vehicle, following the guidance resulted in climbing in thermal lift (Fig. 14). Further tuning of the variometer could improve the performance, but ThermalFinder works now as a reasonable thermal centering pilot aid.

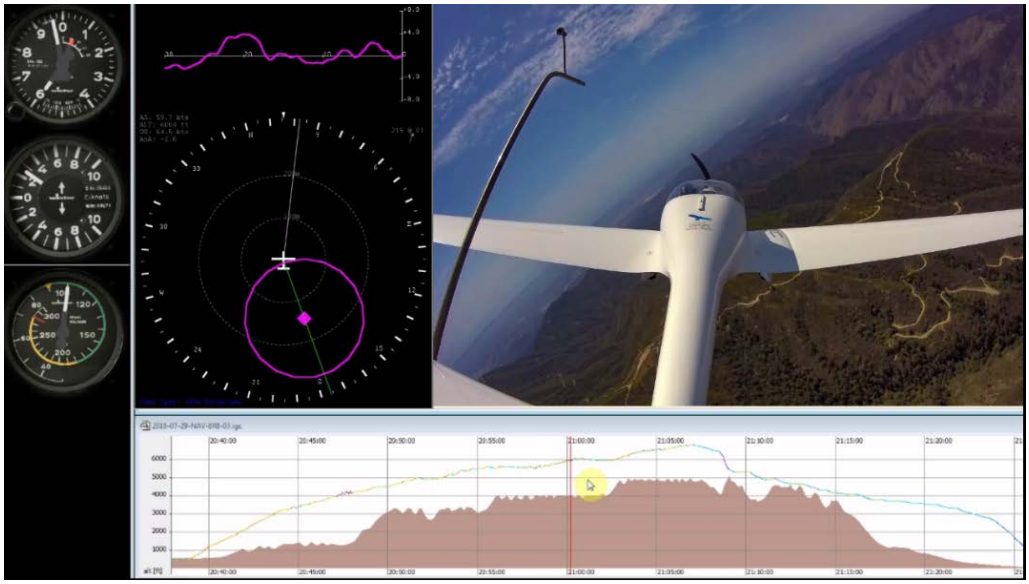

Fig. 14—ThermalFinder again indicating an estimated thermal behind the aircraft

CONCLUSIONS

Two aircraft, one with a mass of 0.410 kg and the other of 710 kg, were flight tested with the same autonomous soaring algorithms. Despite three orders of magnitude difference in weight, both aircraft showed successful closed-loop autonomous soaring guidance. In the smaller unmanned aircraft, the autopilot closed the guidance loop; in the manned aircraft, the pilot closed the guidance loop using commands from a flight director application called ThermalFinder.

The variometer math was discovered to be overcompensated in the 710 kg aircraft (showed inverse "stick thermal" response) and tracked down to angle-of-attack estimate exacerbated by a linear multiplier on airspeed. However, steady-state performance was shown to have less time lag than an Oudie variometer, and was unaffected by motor on/off or glide polar.

These flights show the applicability of the soaring algorithms to solar-battery-electric- and internal combustion engine-powered flight. The variometer and thermal identification algorithms are the key elements of this system, with implementation varying to suit the size and capability of the aircraft. Autonomous soaring holds great potential to increase endurance (and range) or reduce fuel consumption of soaring aircraft. These techniques are applicable to a broad range of aircraft sizes.

ACKNOWLEDGEMENTS

The authors would like to thank the NRL 6.2 Solar Soaring Base Program for funding the NRL portion of this effort.

REFERENCES

1. D. Edwards, "Implementation Details and Flight Test Results of an Autonomous Soaring Controller," presented at the AIAA Guidance, Navigation, and Control Conference and Exhibit, 2008.

2. M. Allen and V. Lin, "Guidance and Control of an Autonomous Soaring Vehicle with Flight Test Results," presented at the 45th AIAA Aerospace Sciences Meeting and Exhibit, 2007.

3. N. Depenbusch, J. Bird, and J. Langelaan, "The AutoSOAR Autonomous Soaring Aircraft Part 2: Hardware Implementation and Flight Results," *Journal of Field Robotics* **35**(4), 435–458 (2018).

4. K. Andersson, I. Kaminer, and K. Jones, "Autonomous Soaring: Flight Test Results of a Thermal Centering Controller," presented at the AIAA Guidance, Navigation, and Control Conference, 2010.

5. D. Edwards and L. Silverberg, "Autonomous Soaring: The Montague Cross Country Challenge," AIAA *Journal of Aircraft*, **47**(5), 1763–1769 (2010), doi:10.2514/1.C000287.

6. D. Parry, "NRL Tests Autonomous 'Soaring with Solar' Concept," Naval Research Laboratory, Washington, DC, [https://www.nrl.navy.mil/news/releases/nrl-tests-autonomous-soaring-solar-concept] accessed 2018-12-14.

7. N. Depenbusch and J. Langelaan. "Coordinated Mapping and Exploration for Autonomous Soaring," Proceedings of Infotech@ Aerospace, March 29–31, 2011, St. Louis, MO, https://doi.org/10.2514/6.2011-1436.

8. A. Noth, "Modeling and Flying Thermal Tubes with an UAV," ETH Zurich, Zurich, Thesis Report (2007).

9. D. Edwards, "Integrating Hydrogen Fuel Cell Propulsion and Autonomous Soaring Techniques," presented at the AIAA Guidance, Navigation, and Control Conference, 2018.

10. A. Kahn, "Atmospheric Thermal Location Estimation," *Journal of Guidance, Control, and Dynamics* **40**(9), 2363–2369 (2017).

11. J. Wharington, “Autonomous Control of Soaring Aircraft by Reinforcement Learning,” Ph.D. dissertation, Royal Melbourne Institute of Technology, 1998.